Electrochimica Acta 299 (2019) 339–345

Contents lists available at ScienceDirect

Electrochimica Acta

journal homepage: www.elsevier.com/locate/electacta

Facile fabrication of open-ended TiO_2 nanotube arrays with large area for efficient dye-sensitized solar cells

Wen Zhu [a], Yanchun Liu [b, c], Aihua Yi [a], Mingshan Zhu [d, **], Wenfang Li [a, b], Nianqing Fu [b, *]

[a] School of Mechanical Engineering, Dongguan University of Technology, Dongguan, Guangdong, 523000, PR China
[b] School of Materials Science and Engineering, South China University of Technology, Guangzhou 510640, PR China
[c] The Key Laboratory of Energy-Efficient Functional Ceramics and Applied Technology of Guangdong Province, Guangzhou Redsun Gas Applications Co., LTD, Guangzhou, 510435, PR China
[d] School of Environment, Jinan University, Guangzhou 510632, PR China

ARTICLE INFO

Article history:
Received 23 September 2018
Received in revised form
2 January 2019
Accepted 4 January 2019
Available online 6 January 2019

Keywords:
Dye-sensitized solar cell
TiO_2 nanotube array
Open-ended
Mechanical grinding
Large area

ABSTRACT

In the present work, we introduce a facile mechanical approach for fast removal of closed bottom-caps of anodized TiO_2 nanotube arrays (TNTAs) to fabricate open-ended TiO_2 nanotube arrays (O-TNTAs). The end-opening process is carried out by mechanically grinding the closed ends on an abrasive paper for a short time of around 15 s. $TiCl_4$ treatment is conducted prior to the opening process to not only enhance the interaction among tubes but also improve surface area of the obtained O-TNTAs membranes. Surface homogeneous, flat and mechanically robust O-TNTAs films with through-hole can be obtained over a large area. The obtained films are exploited as photoanodes for front-illuminated dye-sensitized solar cells. Compared with the close-ended TiO_2 nanotube arrays (C-TNTAs) based device, the solar cell based on O-TNTAs yields an impressive solar power conversion efficiency of 7.7% under one sun illumination, corresponding to a 66% enhancement. The improved cell performance results from both the enhanced light-harvesting and promoted charge collection. The developed through-hole membranes are also favorable for many other potential applications, such as bioinfiltration, flow-through photocatalytical reactors, growth templates and sensors.

1. Introduction

Dye-sensitized solar cells (DSSCs), which possess major advances of easy-fabrication, low-cost, high-efficiency and environmental-friendly, have emerged as a powerful photovoltaic technology. Thanks to the enormous research efforts focusing on developing new pigments (Y123, ADEKA-1, LEG4, *etc.*), efficient redox shuttles (Cu^{+}/Cu^{2+} and Co^{2+}/Co^{3+}, besides I^{-}/I_3^{-}), and electrode/device structure optimization as well, [1–7] the power conversion efficiency (PCE) of DSSCs has so far reached 14.3% under one sun of AM 1.5G illumination [1,2]. Importantly, DSSCs are demonstrated to perform better under weak light [3,7], an PCE of 32% was recently achieved under light-intensity of 1000 lux [7]. The photoanode, commonly composing of a TiO_2 scaffold, of a DSSC takes charge of anchoring dyes and transporting the photo-generated electrons to the current collector. Therefore, efficient electron transport is one of the most favorable properties of a photoanode, apart from high specific surface area [8–15]. Well-ordered one-dimensional TiO_2 nanotube arrays (TNTAs), commonly achieved by anodization, perform excellently in electron transport in DSSCs, keeping more than 90% of charge collection efficiency even with a film thickness up to tens of micrometers [15–21].

The anodized TNTAs feature hexagonal-close-packed and close-ended nanotubes. These closed-ends will block mass (such as dyes and electrolyte) diffusion [22]. Besides application in DSSCs, free-standing TNTAs membranes with through-hole (open-ended) structure would also be favorable for extensive applications such as bioinfiltration, flow-through photocatalytical reactions, sensors, and deposition templates [16,23–27]. Additionally, the barrier layer of the closed caps would hinder the electron transport, degrading the performance of a DSSC [28–30]. Poor interface interaction is commonly formed when bonding the close-ended bottoms onto a secondary electrode using TiO_2 nanoparticles (NPs) as a binding layer, which hampers the efficient electron transfer from TNTAs to

* Corresponding author.
** Corresponding author.
E-mail addresses: mingshanzhu@yahoo.com (M. Zhu), msnqfu@scut.edu.cn (N. Fu).

https://doi.org/10.1016/j.electacta.2019.01.021
0013-4686/

the TiO_2 NPs layer and leads to electron accumulation and thus recombination at the interface [29,30]. Moreover, this interface also causes front-surface light reflection, leading to considerably directed energy loss [22]. Therefore, removing of the closed-ends is of great importance to achieve a device with improved performance [28–33].

To open the closed bottoms, Wang and co-workers developed a potential-shocking technique which introduces a large voltage pulse (180 V) at the end of anodization process [26]. Lin et al. reported a two-step anodization method by subjecting a pre-annealed (200 °C) TNTAs to a 2nd anodization [34]. However, the peeling-off process is tedious and the NTNAs membrane is prone to splinter into small pieces. Wet chemical etching is another effective method to produce open-ended TNTAs (O-TNTAs) apart from electrochemical techniques. Albu et al. exposed the closed bottom of freestanding TNTAs to HF vapors to remove the closed ends [23]. This process involves the use of HF which is toxic to human body and also environmentally unfriendly. By replacing HF with HCl, H_2O_2 or oxalic acid solution, many approaches were successfully developed to prepare O-TNTAs [22,27,33,35]. However, there are some inherent disadvantages of the wet chemical etching process. Firstly, this process is an isotropic etching treatment occurred not only at the closed bottoms but also at any surface exposed to the solution, which might result in inhomogeneity or even destruction of the TNTAs [29]. More importantly, it is commonly observed that the plat wet TNTAs membrane is prone to fracture and then curl into tight rings upon air drying [26], limiting the size of device for future applications. To address the aforementioned problems, Li and co-workers developed a dry-etching technique by bombarding the closed bottoms with highly dense plasma [29]. However, this procedure requires not only special equipment but also harsh processing condition, impeding the extended low-cost application. Therefore, there is still great challenge in preparing flat and mechanically robust TNTAs membranes over large area through facile approaches.

Here we report a simple strategy for the fabrication of freestanding O-TNTAs membrane over large size, *via* a mechanical grinding. In contrast to the isotropic wet chemical approaches, our method provides an anisotropic technique to open the closed-ends of TNTAs without employing any harmful chemicals and the potential destruction of arrays can also thus be avoided. The resulting DSSCs based on the obtained O-TNTAs yield a PCE up to 7.7%.

2. Experimental

2.1. Fabrication of C-TNTAs

The freestanding C-TNTAs membranes were fabricated through a typical anodization method [15,36]. Ti foil (Sigma Aldrich, thickness 0.25 mm, 99.99%) was ultrasonically cleaned by detergent, acetone and DI water in sequence prior to use. The well-cleaned Ti foil with a typical size of 1×5 cm^2 was served as anode and a Pt foil with similar size was employed as cathode. The distance between the anode and cathode is 3 cm. During the anodization, the temperature of anodic cell was kept at around 25 °C by a water-cooling system. The Ti sheet was pre-anodized in an ethylene glycol (EG) solution containing 0.5 wt% NH_4F and 3 vol% DI water at 60 V for 2 h. The resulting TiO_2 film was removed by ultrasonication in DI water to achieve a textured surface. The treated substrate was then subjected to a 2nd anodization in the same condition for 1.5 h. The obtained TNTAs electrodes were annealed at 450 °C for 1 h. The sintered electrodes were subjected to a 0.1 M $TiCl_4$ treatment at 70 °C for 30 min followed by another annealing with the same procedure. The pretreated TNTAs electrode was anodized again in the same condition for 10 min and then emerged in 30 wt% H_2O_2 solution for around 60 s to detach the C-TNTAs from the Ti sheet to form the freestanding C-TNTAs.

2.2. Fabrication of open-ended TNTAs

The freestanding C-TNTAs were attached onto a stainless steel mould with the closed bottom upwards, employing a hot-melted paraffin (80 °C) as binder. During the solidification of the paraffin, a polished silicon wafer was pressed on the sample to enable a flat attachment of C-TNTAs membrane onto the mould. The fixed membrane was gently abraded on an abrasive paper (3000 mesh). The abrading direction of each grinding-cycle (5 times of grinding as one cycle) is perpendicular to each other. As an alternative, the manual grinding can also be replaced by machine grinding using a polisher (operating at around 100 rpm). The grinded TNTAs film was detached form the mould and the paraffin was removed by emerging the film in hot acetone (50 °C) or sintering at 500 °C.

2.3. Device fabrication and characterization

Prior to TNTAs film transfer, a ~2 μm TiO_2 nanoparticular thin-layer was coated on the transparent FTO substrate by a doctor-blading method, using a TiO_2 NPs paste (Dyesol, 18NR-T, ~20 nm in nanoparticle diameter). The obtained TNTAs were cut into designed small pieces by a blade and stamped onto the wet TiO_2-NPs binding layer, followed by a sintering at 450 °C for 1 h. Electrodes which cool down to ~80 °C were sensitized in 0.5 mM N719 dye/ethanol solution overnight and then sandwiched with a sputtered Pt counter electrode to assemble the DSSCs. The electrolyte composes of 0.5 M LiI, 0.05 M I_2, 0.3 M 1-methyl-3-hexylimidazolium iodide (HMII), 0.3 M *N*-methylbenzimidazole (NMB), and 0.5 M 4-*tert*-butylpyridine in 3-methoxypropionitrile. The active area of the devices is 0.16 cm^2.

The morphology of TNTAs were observed by a field-emission scanning electron microscope (Merlin 1530). *J–V* characteristics of DSSCs were measured using a digital source meter (Keithley 2420) under AM 1.5 G illumination (100 mW cm^{-2}) supplied by a Newport-Oriel solar simulator (Model 69911) which was calibrated using a silicon reference cell (NIST). Reverse scan (from 1.0 V to −0.1 V, 50 mV/s) was adopted for collecting the *J–V* curves. The Electrochemical impedance spectroscopy (EIS) was collected at a bias of −0.5 V in the dark, employing a Solartron 1255B frequency response analyzer and a Solartron SI 1287 electrochemical interface system. An ac perturbation signal of an amplitude 10 mV was applied during the EIS measurements and the frequency range was 100 kHz–0.1 Hz.

3. Result and discussion

The preparation of freestanding O-TNTAs films includes two major steps, fabricating of freestanding C-TNTAs membranes and removing of the closed ends by mechanical grinding, as sketched in Fig. 1. Mechanically robust C-TNTAs were obtained over large area by a combined process of multi-step anodization, $TiCl_4$-treatment and detachment (details in Experimental Section). After that, the C-TNTAs membrane was attached onto a stainless steel mould and grinded gently on a DI water-wetted abrasive paper to remove the closed bottoms. Fig. 2a illustrates the bottom surface of pristine C-TNTAs with closed ends. The diameter of the nanotube is around 160 nm. The periods of mechanical grinding were selected to be 0, 5, 10 and 15 s. As illustrated in the SEM images (Fig. 2), the closed ends of nanotubes were removed gradually by increasing the grinding time. A homogenously and thoroughly open-ended morphology of O-TNTAs was obtained with 15 s of grinding (Fig. 2d).

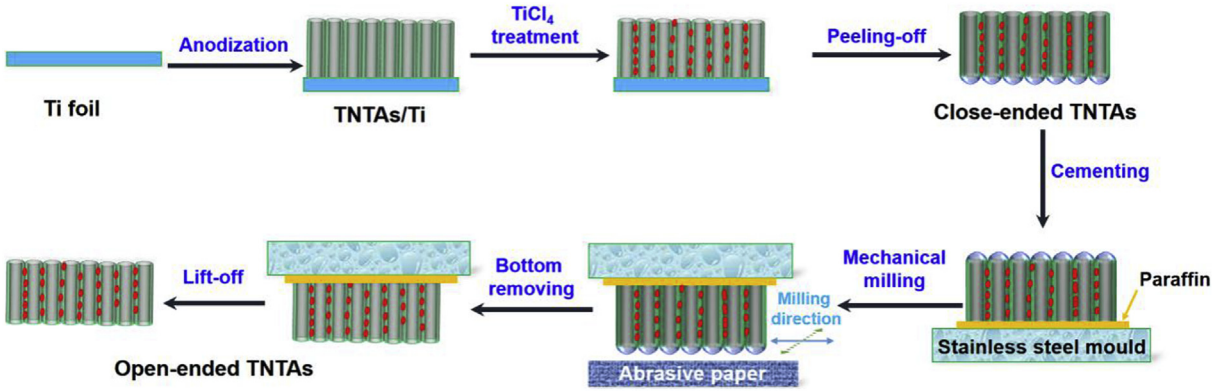

Fig. 1. Schematic representation of the procedure used to fabricate the freestanding open-ended TiO_2 nanotube arrays (TNTAs), including the preparation of close-ended TNTAs by multi-anodization and mechanical grinding of the closed cap layer on an abrasive paper.

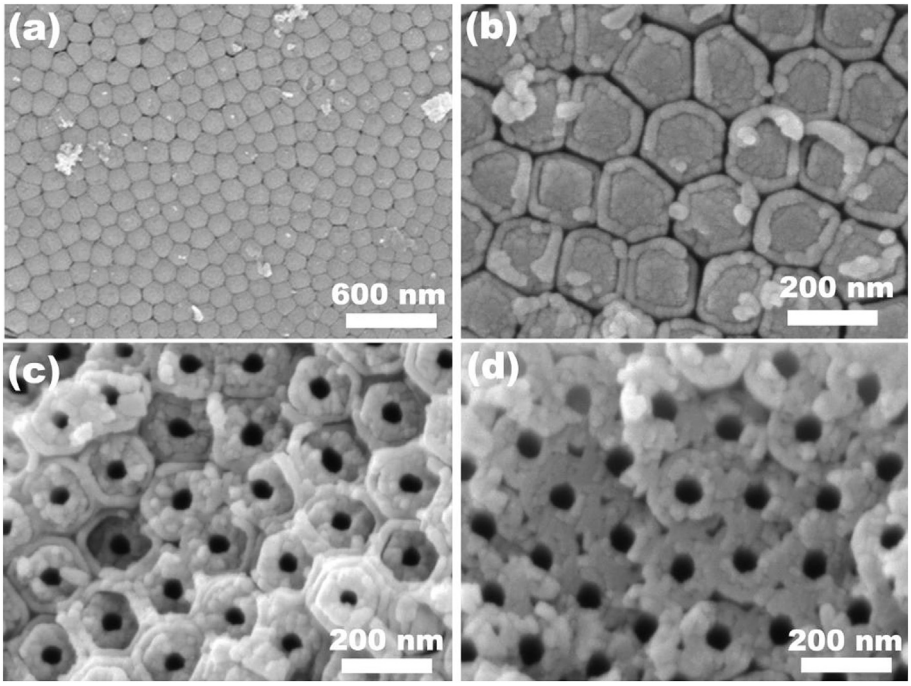

Fig. 2. Bottom-viewed SEM images of a) close-ended TNTAs and b-d) open-ended TNTAs prepared by mechanical grinding with a grinding period of 5, 10 and 15 s, respectively.

In the developed approach, the $TiCl_4$-treatment before C-TNTAs peeling off plays a significant role in enhancing the interaction between individual nanotubes, as shown in Fig. 3a and b. This is because the small TiO_2 particles can be formed at any available surface of TNTAs by $TiCl_4$ hydrolysis to weld the adjacent nanotubes. The improved mechanical interlock among nanotubes enables the formation of mechanically robust and non-curled O-TNTAs membranes with desirable size, depending on the size of C-TNTAs by anodization (Fig. 3c and d). Additionally, the $TiCl_4$-treatment also increases the surface area to improve dye-loading amount for enhanced light-harvesting and thus cell efficiency [15,37,38].

Three types of photoanode, namely the C-TNTAs film with top surface (opened surface) upright (C-TNTAs T-up), O-TNTAs with top surface upright (O-TNTAs T-up) and O-TNTAs with bottom surface upright (O-TNTAs B-up), were constructed to estimate the performance of obtained TNTAs films in DSSCs. The device architectures are schematically illustrated in Fig. 4a. Photocurrent density-voltage curves (*J-V*) of the corresponding DSSCs are shown in Fig. 4b and detailed photovoltaic parameters are summarized in Table 1. To understanding the contribution of the TiO_2-NPs binding layer to the cell performance, device with only NPs film (2 μm) was also prepared and tested as a control, giving a total PCE of 2.5%. For T-up structured devices with C-TNTAs, the short-circuit current density (J_{sc}), the open-circuit voltage (V_{oc}), and the fill factor (*FF*) are 10.1 mA cm^{-2}, 0.68 V, and 0.67, respectively, giving an efficiency of 4.6% at a tube length of around 18 μm. After the removal of closed bottoms, the J_{sc} improves considerably to 14.2% mA cm^{-2} while the V_{oc} also increases from 0.68 to 0.71 V. As a result, a remarkably greater PCE of 6.9% is yielded for the O-TNTAs based device with T-up structure. By inverting the O-TNTAs film to form a B-up architecture, the PCE of the resulting cell is further improved to 7.7%, resulting mainly from the additionally enhanced J_{sc} of 15.5 mA cm^{-2}. This PCE is even much higher than that of the DSSC with a 20 μm TiO_2-NPs-film based photoanode (Table 1, note that 20 μm may not be the optimized thickness for efficient DSSCs based

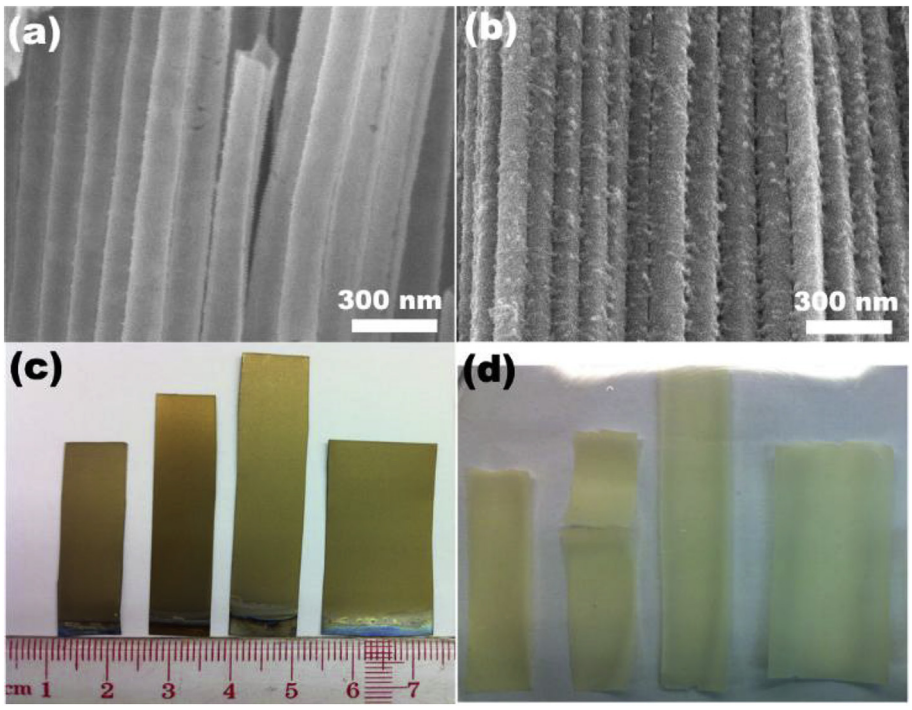

Fig. 3. Cross-section viewed SEM images of the a) as prepared TiO_2 nanotube arrays (TNTAs) and b) $TiCl_4$ treated TNTAs, showing the enhanced interaction among the individual tubes. Digital images of c) as prepared TNTAs/Ti electrodes and d) freestanding open-ended TNTAs membranes with various size.

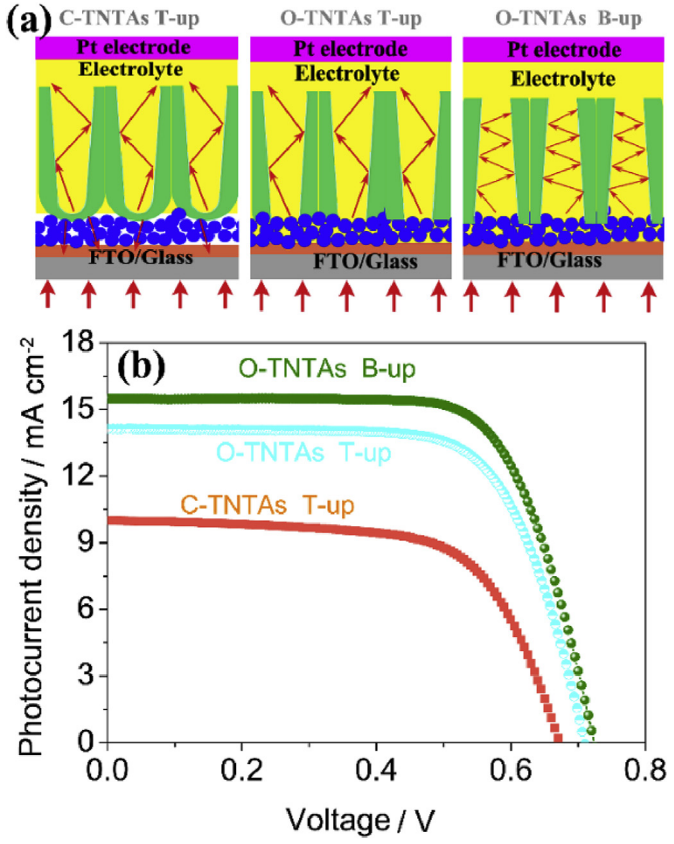

Fig. 4. a) Schematic illustration of DSSCs with various TiO_2 photoande architectures. b) Photocurrent-voltage characteristic curves of DSSCs measured under 100 mW cm^{-2} of AM1.5G illumination.

on TiO_2-NPs photoanode). The enhanced light-harvesting might be one of the factors contributed to the improved J_{sc} of B-up based device. Because the nanotubes derived from the EG electrolyte feature a hollow conical columnar structure and the inverted electrode architecture (B-up) will induce a more pronounced light-trapping effect for enhanced light absorption [39,40], as schematically illustrated in Fig. 4a.

As listed in Table 1, the dye-loading amount among various TNTAs based devices shows only small difference. The significantly greater J_{sc} of the O-TNTAs based devices compared with that of C-TNTAs based cells is not interpretable according to the effect of dye loading. The optical property of the photoanodes was therefore conducted to study any reasons for the improved J_{sc} and PCE of the DSSCs. As schematically represented in Fig. 5a and b, the bottom surface of C-TNTAs with compactly packed closed-ends might cause front light-reflection when the closed bottoms were faced to TiO_2 binding layer to build the photonaode for front-illuminated DSSCs. The digital image displayed in Fig. 5 c (right panel) clearly shows the colorful interferometry fringe of the reflected light at the bottom surface of C-TNTAs while no observable reflection interference can be found on the bottom surface of O-TNTAs (left panel). Compared with the C-TNTAs, the UV–Vis transmission spectra shown in Fig. 5d demonstrate a remarkably enhanced luminousness of the O-TNTAs electrode, especially at shorter wavelength range of 350–600 nm where the N719 dyes possess strong light-extinction. Because the incident light with shorter wavelength is more prone to be reflected. The photograph shown as inset of Fig. 5d also confirms the improved transparency of O-TNTAs electrode. The decreased front light-reflection will reduce the direct energy loss and increase the light utilization consequently. As a result, an improvement in J_{sc} and PCE can be thus obtained.

To understand further factor for the enhanced device performance, electrochemical impedance spectroscopy (EIS), conducted at a moderate bias potential of −0.5 V in the dark, was measured to reveal the charge transport behavior within the devices. The

Table 1
Photovoltaic characteristics of the DSSCs based on various TiO_2 photoanodes and different device architectures.

Devices	d[a]/μm	Device type	Dye-loading/$\times 10^{-7}$ mol cm^{-2}	J_{sc}/mA cm^{-2}	V_{oc}/V	*FF*	η/%
TiO_2 NPs	2	NA	0.31	4.3	0.76	0.77	2.5
TiO_2 NPs	20	NA	3.2	18.1	0.57	0.63	6.5
C-TNTAs	18 + 2	T-up	1.1	10.1	0.68	0.67	4.6
O-TNTAs	18 + 2	T-up	1.2	14.2	0.71	0.68	6.9
O-TNTAs	18 + 2	B-up	1.2	15.5	0.72	0.69	7.7

[a] Thickness of the TiO_2 films. The TNTAs were structured on a 2 μm thick TiO_2 NPs binder layer.

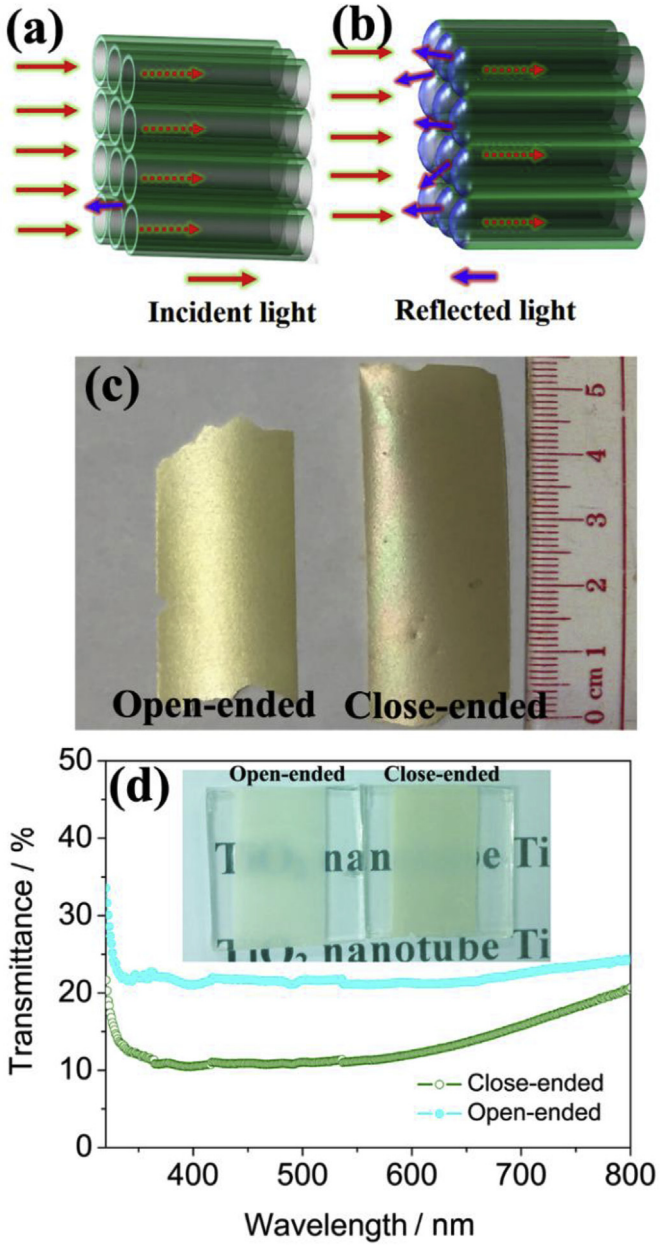

Fig. 5. Schematic illustration of the light reflection at the bottom surface of a) open-ended TNTAs and b) close-ended TNTAs with regular packed caps. c) Digital photographs comparing the interferometry fringe of reflected light at the bottom surface of two kinds of TNTAs. d) Transmission spectra of the close-ended TNTAs and open-ended TNTAs based electrodes. The inset showing the digital images of the two electrodes

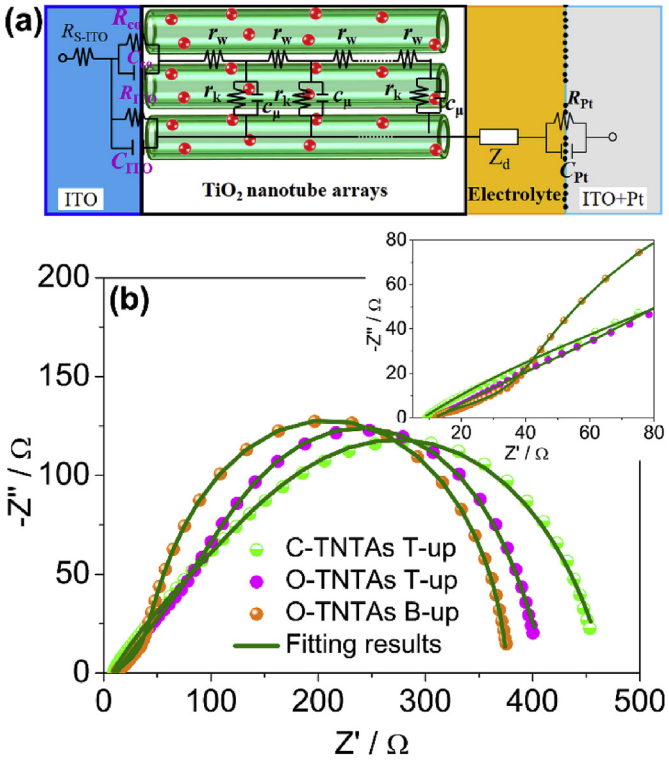

Fig. 6. a) The equivalent circuit of the completed DSSCs represented by a transmission line model. b) Nyquist plots of the corresponding DSSCs, measured at a bias of −0.5 V in the dark. The inset of b) shows the magnification of the high frequencies region of the Nyquist plots.

corresponding results are shown in Fig. 6 and the concerned parameters are extracted by fitting the EIS results, according to the equivalent circuits represented by a transmission line model (Fig. 6a). More details for data extraction and calculation can be found in reported works [9,12,41–43]. The electron transport resistance, R_w ($=r_w{}^*L$, where L is the thickness of the TiO_2 film), within the TiO_2 films is tested to be 141.2, 74.3 and 32.8 Ω for the C-TNTAs T-up, O-TNTAs T-up and O-TNTAs B-up based DSSCs, respectively. The removal of impurity enriched barrier layer (mainly closed bottoms) of C-TNTAs will facilitate the electron transfer from TNTAs to NPs layer, since the impurities will scatter the electron diffusion. Additionally, the hollow conical columnar-structure of nanotubes with larger inner diameter at top (than at bottom) enables TiO_2 particles in binding layer easily to enter into the nanotube (top surface pores) and forms a reinforced interfacial interlock in B-up structure. In contrast, the interaction between NPs and overlying O-TNTAs with T-up structure is relative poor, due to the limited contact area. The enhanced bonding strength between O-TNTAs and NPs is evidenced by the SEM images shown in Fig. S1, apparent interfacial gaps between the TNTAs and NPs binder layer are formed for both the C-TNTAs and O-TNTAs electrodes with T-up structure due to the stress occurred during SEM sample preparation by mechanical cutting. Owing to the removal of impurity enriched

Table 2
Electron transport characteristics extracted from the electrochemical impedance spectra results shown in Fig. 6.

Devices	d[a]/μm	Device type	R_w/Ω	R_k/Ω	η_{cc}/%
C-TNTAs	18 + 2	T-up	141.2	308.4	68.6
O-TNTAs	18 + 2	T-up	74.3	318.3	81.1
O-TNTAs	18 + 2	B-up	32.8	330.5	90.9

barrier layer and formation of compacted interface, the O-TNTAs based devices demonstrates fast electron transport and increased interfacial recombination resistance ($R_k = r_k{}^*L$, Table 2) at the TiO_2/electrolyte interface and thus an alleviative charge recombination, which is consistent with the increased V_{oc} of O-TNTAs based devices. The C-TNTAs based DSSC shows a low charge collection efficiency, η_{cc} (=1-R_w/(R_k + R_w)), of 68.6%, this value increases to 81.1% by removing the closed caps. The O-TNTAs based DSSC with B-up architecture shows the highest η_{cc} value of 90.9%. This result keeps in line with the observed cell performance in that the O-TNTAs based device with B-up structure yields the best J_{sc} and highest PCE, indicating that the improved η_{cc} of the O-TNTAs based device, especially the B-up ones, contributes to the impressive enhancement in performance, besides the optical factors aforementioned.

4. Conclusion

In summary, we develop a new mechanical approach for facile fabrication of open-ended TiO_2 nanotube arrays over a large area. The tube-opening process can be completed in a time scale of 10 s, without involving any precision equipment and harmful chemicals. The obtained freestanding O-TNTAs film is exploit as photoanode in front-illuminated DSSCs and the resulting device yields an impressive PCE of 7.7%. The improved performance of O-TNTAs based device arises from both the enhanced optical properties (decreased front light reflection and improved light-trapping within nanotubes) and promoted electron collection efficiency. The developed sizable O-TNTAs membranes can be applied to extended TNTAs applications, such as bioinfiltration, flow-through photocatalytical reactions and sensors.

Acknowledgement

This work was financially supported by National Natural Science Foundation of China (Grants No. 61604058), the Fundamental Research Funds for the Central Universities (2017MS003), and the Natural Science Foundation of Guangdong Province (Grant No. 2018A030310024).

Appendix A. Supplementary data

Supplementary data to this article can be found online at https://doi.org/10.1016/j.electacta.2019.01.021.

References

[1] M.A. Green, Y. Hishikawa, E.D. Dunlop, D.H. Levi, J. Hohl-Ebinger, A.W.Y. Ho-Baillie1, Solar cell efficiency tables (Version 52), Prog. Photovolt. Res. Appl. 26 (2018) 427–436.
[2] K. Kakiage, Y. Aoyama, T. Yano, K. Oya, J.I. Fujisawa, M. Hanaya, Highly efficient dye-sensitized solar cells with collaborative sensitization by silyl-anchor and carboxy-anchor dyes, Chem. Commun. 51 (2015) 15894–15897.
[3] M. Freitag, J. Teuscher, Y. Saygili, X. Zhang, F. Giordano, P. Liska, J. Hua, S.M. Zakeeruddin, J.E. Moser, M. Grätzel, A. Hagfeldt, Dye-sensitized solar cells for efficient power generation under ambient lighting, Nat. Photon. 11 (2017) 372–378.
[4] E. Benazzi, M. Magni, A. Colombo, C. Dragonetti, S. Caramori, C.A. Bignozzi, R. Grisorio, G.P. Suranna, M.P. Cipolla, M. Manca, D. Roberto, Bis(1,10-phenanthroline) copper complexes with tailored molecular architecture: from electrochemical features to application as redox mediators in dye-sensitized solar cells, Electrochim. Acta 271 (2018) 180–189.
[5] J. Cong, D. Kinschel, Q. Daniel, M. Safdari, E. Gabrielsson, H. Chen, P.H. Svensson, L. Sun, L. Kloo, Bis(1,1-Bis(2-Pyridyl) ethane) copper(I/II) as an efficient redox couple for liquid dye-sensitized solar cells, J. Mater. Chem. 4 (2016) 14550–14554.
[6] Y. Bai, Q. Yu, N. Cai, Y. Wang, M. Zhang, P. Wang, High-efficiency organic dye-sensitized mesoscopic solar cells with a copper redox shuttle, Chem. Commun. 47 (2011) 4376–4378.
[7] Y. Cao, Y. Liu, S.M. Zakeeruddin, A. Hagfeldt, M. Grätzel, Direct contact of selective charge extraction layers enables high-efficiency molecular photovoltaics, Joule 2 (2018) 1108–1117.
[8] J.S. Shaikh, N.S. Shaikh, S.S. Mali, J.V. Patil, K.K. Pawar, P. Kanjanaboos, C.K. Hong, J.H. Kimd, P.S. Patil, Nanoarchitectures in dye-sensitized solar cells: metal oxides, oxide perovskites and carbon-based materials, Nanoscale 10 (2018) 4987–5034.
[9] N. Tetreault, M. Gräetzel, Novel nanostructures for next generation dye-sensitized solar cells, Energy Environ. Sci. 5 (2012) 8506–8516.
[10] H.Y. Chen, Y.F. Xu, D.B. Kuang, C.Y. Su, Recent advances in hierarchical macroporous composite structures for photoelectric conversion, Energy Environ. Sci. 7 (2014) 3887–3901.
[11] W.Q. Wu, H.L. Feng, H.Y. Chen, D.B. Kuang, C.Y. Su, Recent advances in hierarchical three-dimensional titanium dioxide nanotree arrays for high-performance solar cells, J. Mater. Chem. 5 (2017) 12699–12717.
[12] N. Fu, C. Huang, Y. Liu, X. Li, W. Lu, L. Zhou, F. Peng, Y.C. Liu, H. Huang, Organic-free anatase TiO2 paste for efficient plastic dye-sensitized solar cells and low temperature processed perovskite solar cells, ACS Appl. Mater. Interfaces 7 (2015) 19431–19438.
[13] Z. Xu, X. Yin, Y. Guo, Y. Pu, M. He, Ru-doping in TiO2 electron transport layers of planar heterojunction perovskite solar cells for enhanced performance, J. Mater. Chem. C 6 (2018) 4746–4752.
[14] C. Huang, P. Lin, N. Fu, K. Sun, M. Ye, C. Liu, X. Zhou, L. Shu, X. Hao, B. Xu, X. Zeng, Y. Wang, S. Ke, Ionic liquid modified SnO2 nanocrystals as a robust electron transporting layer for efficient planar perovskite solar cells, J. Mater. Chem. (2018), https://doi.org/10.1039/C8TA04131H.
[15] N. Fu, Y. Liu, Y.C. Liu, W. Lu, L. Zhou, F. Peng, H. Huang, Facile preparation of hierarchical TiO2 nanowire-nanoparticlenanotube Architecture for highly efficient dye-sensitized solar cells, J. Mater. Chem. 3 (2015) 20366–20374.
[16] K. Lee, A. Mazare, P. Schmuki, One-dimensional titanium dioxide nanomaterials: nanotubes, Chem. Rev. 114 (2014) 9385–9454.
[17] C.T. Yip, H. Huang, L. Zhou, K. Xie, Y. Wang, T. Feng, J. Li, W.Y. Tam, Direct and seamless coupling of TiO2 nanotube photonic crystal to dye-sensitized solar cell: a single-step approach, Adv. Mater. 23 (2011) 5624–5628.
[18] S. Lee, I.J. Park, D.H. Kim, W.M. Seong, D.W. Kim, G.S. Han, J.Y. Kim, H.S. Jung, K.S. Hong, Crystallographically preferred oriented TiO2 nanotube Arrays for efficient photovoltaic energy conversion, Energy Environ. Sci. 5 (2012) 7989–7995.
[19] A. Elzarka, N. Liu, I. Hwang, M. Kamal, P. Schmuki, Chem. Eur. J. 23 (2017) 12995–12999.
[20] W.C. Chen, M.H. Yeh, L.Y. Lin, R. Vittal, K.C. Ho, Double-wall TiO2 nanotubes for dye-sensitized solar cells: a study of growth mechanism, ACS Sustain. Chem. Eng. 6 (2018) 3907–3915.
[21] J.R. Jennings, A. Ghicov, L.M. Peter, P. Schmuki, A.B. Walker, Dye-sensitized solar cells based on oriented TiO2 nanotube Arrays: transport, trapping, and transfer of electrons, J. Am. Chem. Soc. 130 (2008) 13364–13372.
[22] C.J. Lin, W.Y. Yu, S.H. Chien, Transparent electrodes of ordered opened-end TiO2-nanotube Arrays for highly efficient dye-sensitized solar cells, J. Mater. Chem. 20 (2010) 1073–1077.
[23] S.P. Albu, A. Ghicov, J.M. Macak, R. Hahn, P. Schmuki, Self-organized, free-standing TiO2 nanotube membrane for flow-through photocatalytic applications, Nano Lett. 7 (2007) 1286–1289.
[24] O.K. Varghese, M. Paulose, T.A. LaTempa, C.A. Grimes, High-rate solar photocatalytic conversion of CO2 and water vapor to hydrocarbon fuels, Nano Lett. 9 (2009) 731–737.
[25] M. Paulose, L. Peng, K.C. Popat, O.K. Varghese, T.J. LaTempa, N. Bao, T.A. Desai, C.A. Grimes, Fabrication of mechanically robust, large area, polycrystalline nanotubular/porous TiO2 membranes, J. Membr. Sci. 319 (2008) 199–205.
[26] D. Wang, L. Liu, Continuous fabrication of free-standing TiO2 nanotube Array membranes with controllable morphology for depositing interdigitated heterojunctions, Chem. Mater. 22 (2010) 6656–6664.
[27] C.J. Lin, W.Y. Yu, Y.T. Lu, S.H. Chien, Fabrication of open-ended high aspect-ratio anodic TiO2 nanotube films for photocatalytic and photoelectrocatalytic applications, Chem. Commun. 45 (2008) 6031–6033.
[28] C. Rho, J.H. Min, J.S. Suh, Barrier layer effect on the electron transport of the dye-sensitized solar cells based on TiO2 nanotube arrays, J. Phys. Chem. C 116 (2012) 7213–7218.
[29] L.L. Li, Y.J. Chen, H.P. Wu, N.S. Wang, E.W.G. Diau, Detachment and transfer of ordered TiO2 nanotube Arrays for front-illuminated dye-sensitized solar cells, Energy Environ. Sci. 4 (2011) 3420–3425.
[30] J. Choi, S. Song, G. Kang, T. Park, Dye-sensitized solar cells employing doubly or singly open-ended TiO2 nanotube Arrays: structural geometry and charge transport, ACS Appl. Mater. Interfaces 6 (2014) 15388–15394.
[31] J. Choi, Y.S. Kwon, T. Park, Doubly open-ended TiO2 nanotube Arrays

decorated with a few nm-sized TiO2 nanoparticles for highly efficient dye-sensitized solar cells, J. Mater. Chem. 2 (2014) 14380–14385.
[32] C.T. Yip, M. Guo, H. Huang, L. Zhou, Y. Wang, C. Huang, Open-ended TiO2 nanotubes formed by two-step anodization and their application in dye-sensitized solar cells, Nanoscale 4 (2012) 448–450.
[33] J. Choi, S.H. Park, Y.S. Kwon, J. Lim, I.Y. Song, T. Park, Facile fabrication of aligned doubly open-ended TiO2 nanotubes, via a selective etching process, for use in front-illuminated dye sensitized solar cells, Chem. Commun. 48 (2012) 8748–8750.
[34] J. Lin, J. Chen, X. Chen, Facile fabrication of free-standing TiO2 nanotube membranes with both ends open via self-detaching anodization, Electrochem. Commun. 12 (2010) 1062–1065.
[35] J.H. Park, T.W. Lee, M.G. Kang, Growth, detachment and transfer of highly-ordered TiO2 nanotube Arrays: use in dye-sensitized solar cells, Chem. Commun. 25 (2008) 2867–2869.
[36] N. Fu, X. Li, Y. Liu, Y.C. Liu, M. Guo, W. Li, H. Huang, Low temperature transfer of well-tailored TiO2 nanotube Array membrane for efficient plastic dye-sensitized solar cells, J. Power Sources 343 (2017) 47–53.
[37] S. So, I. Hwang, P. Schmuki, Hierarchical DSSC structures based on “single walled” TiO2 nanotube Arrays reach a back-side illumination solar light conversion efficiency of 8%, Energy Environ. Sci. 8 (2015) 849–854.
[38] J. Choi, G. Kang, T. Park, A competitive electron transport mechanism in hierarchical homogeneous hybrid structures composed of TiO2 nanoparticles and nanotubes, Chem. Mater. 27 (2015) 1359–1366.
[39] S. Foster, S. John, Light-trapping in dye-sensitized solar cells, Energy Environ. Sci. 6 (2013) 2972–2983.
[40] W. Zeng, M. Wang, Y. Li, J. Wan, H. Huang, H. Tao, D.L. Carroll, X. Zhao, D. Zou, G. Fang, Semi-closed tubular light-trapping geometry dye sensitized solar cells with stable efficiency in wide light intensity range, J. Power Sources 261 (2014) 75–85.
[41] F. Fabregat-Santiago, J. Bisquert, G. Garcia-Belmonte, G. Boschloo, A. Hagfeldt, Influence of electrolyte in transport and recombination in dye-sensitized solar cells studied by impedance spectroscopy, Sol. Energy Mater. Sol. Cells 87 (2005) 117–131.
[42] Q. Wang, S. Ito, M. Grätzel, F. Fabregat-Santiago, I. Mora-Seró, J. Bisquert, T. Bessho, H. Imai, Characteristics of high efficiency dye-sensitized solar cells, J. Phys. Chem. B 110 (2006) 25210–25221.
[43] M. Adachi, M. Sakamoto, J. Jiu, Y. Ogata, S. Isoda, Determination of parameters of electron transport in dye-sensitized solar cells using electrochemical impedance spectroscopy, J. Phys. Chem. B 110 (2006) 13872–13880.